CHAPTER 17

RAW Quantum transition state theory

G. Mills[a], G. K. Schenter[b], D. E. Makarov[b,c] and H. Jónsson[a,*]

[a] *Department of Chemistry, Box 351700, University of Washington, Seattle, WA 98195-1700*

[b] *Environmental Molecular Sciences Laboratory, Pacific Northwest National Laboratories, Richland, WA 99352*

[c] *University of California Santa Barbara, Santa Barbara, CA 93106*

[*] *To whom correspondance should be addressed, e-mail hannes@u.washington.edu*

Contents

1. – Introduction

Many important problems in chemistry and condensed matter physics involve the characterization of the rate of a transition of atoms and/or electrons. Most transitions observable in the laboratory are 'rare events' in the sense that the transition rate is many orders of magnitude smaller than the rate associated with molecular vibrations. A direct simulation of the atomic scale dynamics is not useful for studying such transitions because the simulated time interval is far too short to include even a single transition. Transition state theory (TST) is well established and widely used for calculating rates of slow transitions in classical systems [1, 2]. It gives an approximate estimate of the rate constant which frequently is accurate enough for practical purposes. It, furthermore, can provide a viable way of computing the exact rate constant because the dynamical corrections to TST can often be readily evaluated from short time trajectories launched from the transition state.

Basically, classical TST transforms the dynamical problem into a statistical one by approximating the transition rate as being proportional to the probability of finding the system in a transition state times a flux factor representing the rate at which the system leaves the transition state in the direction of products,

$$k^{TST} = \frac{\bar{v}}{2} \frac{Q_{cl}^{\ddagger}}{Q_{cl}^{R}} \tag{1}$$

Here, $\bar{v}$ is the average velocity, Q_{cl}^{R} is the classical reactant partition function,

$$Q_{cl}^{R} = \frac{1}{N!} \left(\frac{2\pi\mu kT}{h^2}\right)^{3N/2} \int_R e^{-V(q)/kT} \, d^N q \tag{2}$$

and $Q_{cl}^{\ddagger}$ is the transition state partition function

$$Q_{cl}^{\ddagger} = \frac{1}{N!} \left(\frac{2\pi\mu kT}{h^2}\right)^{3N/2} \int e^{-V(q)/kT} \, \delta(q - q^{\ddagger}) \, d^N q \tag{3}$$

$V(q)$ is the potential energy function and q is an N-dimensional vector of the mass-scaled coordinates of the system. The classical transition state is a N-1 dimensional surface separating the regions of configuration space associated with reactants and products. (This can be generalized to phase space [2, 3]). A good approximation to the rate constant can be obtained from TST if the transition state is chosen to be a dividing surface that represents a tight bottleneck for the advancement of the system from reactants to products. The accuracy of the TST approximation depends strongly on the choice of the dividing surface. For classical systems, it can be shown that TST always gives an overestimate of the rate. This provides a variational principle for optimizing the location of the dividing surface [2, 3]. A convenient way to calculate the variationally optimized rate constant is to evaluate the reversible work of shifting a dividing surface from the

reactant region towards products, identifying on the way the optimal transition state as the dividing surface corresponding to maximum free energy. The free energy change includes both the work of pushing the dividing surface along the reaction path and the work of rotating the dividing surface against the (generalized) torque acting on it [4].

The challenge is to generalize TST to quantum systems. Several experimentally measured transition rates show temperature dependence where below a crossover temperature, T_c, the effective activation energy is significantly reduced and may even vanish [5]. This is characteristic of the onset of quantum behaviour where thermally assisted tunneling becomes the dominant transition mechanism. A purely statistical quantum TST, which does not require calculations of the system's time evolution, is particularly useful for analyzing such transitions since accurate calculations of quantum dynamics can presently only be carried out for low-dimensional systems, short time intervals, or for certain model systems [6, 7].

2. – Feynman path integrals

Several versions of quantum TST have been proposed [2]. The most widely used formulation is based on statistical Feynman path integrals where the canonical partition function of a quantum system is given by [8]

$$Q = (\mu/2\pi\hbar\Delta\tau)^{NP/2} \int e^{-S_E[q(\tau)]/\hbar}\, \mathcal{D}[q(\tau)]. \tag{4}$$

Here S_E is the so called Euclidean action, $S_E = \int_0^{\beta\hbar} H d\tau$ with H being the classical Hamiltonian. The statistical mechanical path integrals are directly related to the path integrals for time evolution of a quantum system and can be obtained by replacing time with an 'imaginary time' $i\tau$ [8]. For discretized paths described by P configurations of the system, the action can be approximated as

$$S_E(\mathbf{q}) = \Delta\tau \sum_{j=1}^{P} \left[\frac{\mu}{2} \left| \frac{q_{j+1} - q_j}{\Delta\tau} \right|^2 + V(q_j) \right] \tag{5}$$

where $\Delta\tau = \beta\hbar/P$ with $\beta = 1/k_B T$ and μ is the scaling mass (boldface type is used here for NP dimensional vectors specifying the configuration of a closed Feynman path with P images, while N dimensional vectors are not boldface). This leads to a mathematical analogy between the partition function of a quantum particle and the classical partition function of a string of P 'images' (or replicas) of the system connected by springs with spring constant that depends on temperature [9]

$$k_{sp} \;=\; \mu P \left(\frac{k_B T}{\hbar} \right)^2 . \tag{6}$$

This discrete path integral formulation becomes exact as $P \to \infty$ [8].

3. – How should a quantum transition state be defined?

While the Feynman path integral formulation provides a practical method for evaluating numerically the statistical mechanical properties of quantum systems in thermodynamic equilibrium, the question arises how this can be used to calculate a transition

rate, and the critical question becomes: How should the quantum transition state be defined? In previous theories, the transition state has been defined in terms of an N-1 dimensional dividing surface in the classical coordinate space just as in classical TST [2]. In particular, in the centroid density method, proposed by Gillan [10] and later generalized by others [11, 12, 13, 14, 4], the transition state constraint is applied to the average, or centroid, of the Feynman paths $q_0 = (1/\beta\hbar)\int_0^{\beta\hbar} q(\tau)d\tau$. This was tested and found to work well for transitions involving symmetric barriers [10, 11, 15].

The centroid constraint, however, does not work well for asymmetric transitions at low temperature [16, 17]. We show an example of that below. We also present here a discussion [18, 19] of a different formulation of a quantum TST where the transition state is defined in a more general way, as a NP-1 dimensional cone in the space of all closed Feynman paths discretized with P images. The theory represents a natural generalization of the so called 'instanton theory' (see below) which is based on a harmonic approximation. The centroid does not play any special role in this new theory. A method for evaluating the free energy barrier in this higher dimensional space, which we will refer to as 'action-space', is described. The technique involves evaluating the reversible work required to shift the system confined to a NP-1 dimensional dividing surface in action-space from the reactant region towards products. We refer to the method as reversible action-space work quantum transition state theory (RAW-QTST). The discussion here will be focused mainly on the methodology and an application to a one-dimensional test problem. An application to a large problem, the associative desorption of H_2 from a $Cu(110)$ surface, has been described elsewhere [18].

4. – The action surface and the minimum action path

We first discuss the motivation for our definition of the quantum transition state. In classical systems, the optimal transition state is a bottleneck region on the way from reactants to products where the probability of finding the system is small, i.e. configurations q where the statistical weight $exp(-V(q)/kT)$ is minimal. In the low temperature limit, the saddle point on the potential energy surface, $V(q)$, is of crucial importance and, in a harmonic limit (i.e. in harmonic TST [28, 29]), the transition rate depends exponentially on the energy difference between the saddle point and the initial state. A direct generalization of these concepts to quantum systems, where the statistical weight of a configuration $\mathbf{q}$ of a closed Feynman path is given by $exp(-S_E(\mathbf{q})/\hbar)$, focuses on the action surface $S_E(\mathbf{q})$ [16] as opposed to the potential energy surface $V(q)$ in the classical case. A logical choice for a quantum transition state is a region in action space where $exp(-S_E(\mathbf{q})/\hbar)$ is small, i.e. where the action $S_E(\mathbf{q})$ is large. This would imply that saddle points on the action surface become dominant regions for determining the transition rate at low temperature. Such saddle points are commonly referred to as 'instantons' and a very successful theory of transition rates at low temperature indeed involves harmonic approximation of $S_E(\mathbf{q})$ in the neighborhood of the saddle points [5].

The topology of the action surface is, therefore, of central importance but is very hard to visualize because of the high dimensionality (NP) even for systems with only one degree of freedom (N=1). Figure 1 shows the potential energy function for a simple, one-dimensional test problem, an asymmetric Eckart barrier. The transition is exoergic by $0.19\,eV$ with a barrier height of $0.25\,eV$ (the functional form and potential parameters are the same as in reference [17]). In order to visualize the action surface with a contour plot, the closed Feynman paths may only include two variables. Rather than represent the paths with two images in real space, it is preferable to go to Fourier space and represent

the paths with two Fourier components $q(\tau) = q_0 + q_1 \sin(2\pi\tau/\beta\hbar)$. The variable q_0 is the average position of the images (the location of the centroid) and the variable q_1 is the lowest order Fourier component representing the extent to which the path stretches away from the centroid location. The action S_E along the line where $q_1 = 0$ is simply proportional to the potential energy, $V(q_0)$. At high temperature (see figure 2a), the action increases as the Feynman paths are stretched out from the centroid ($q_1 \neq 0$), i.e. when quantum delocalization is introduced. This means that the optimal way for the system to go from the reactant region to products is without quantum delocalization, i.e. by classical hopping over the potential barrier. But, below a crossover temperature, T_c (275 K in this case), the topology of the action surface changes as a local maximum of action appears at $q_1 = 0$ in the barrier region (see figure 2b and figure 2c). Then, a smaller action is obtained with open, delocalized paths (see figure 2d). This means that the optimal way for the system to go from the reactant region to products at temperatures below T_c is by taking advantage of quantum delocalization, i.e. by quantum mechanical tunneling. In this low temperature region, saddle points on the action surface appear off the 'classical', collapsed path ($q_1 = 0$) axis.

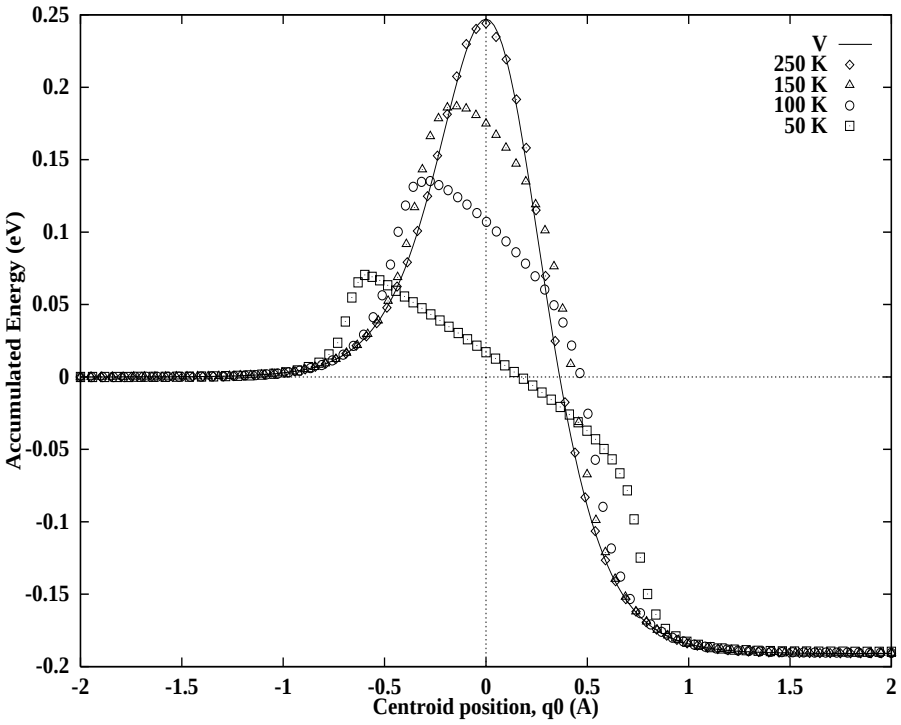

Fig. 1. – The potential energy for a one-dimensional test problem, an asymmetric Eckart barrier. The potential energy is shown with a solid line. The points show the scaled action, $S_E/\beta\hbar$, along the minimum action path at various temperatures. As the temperature is lowered below the crossover temperature, T_c, the springs in the Feynman paths become weaker and the paths open more up near the barrier. The maximum action along the minimum action path (the instanton) is much closer to the reactant region than the product region due to the asymmetry of the potential barrier.

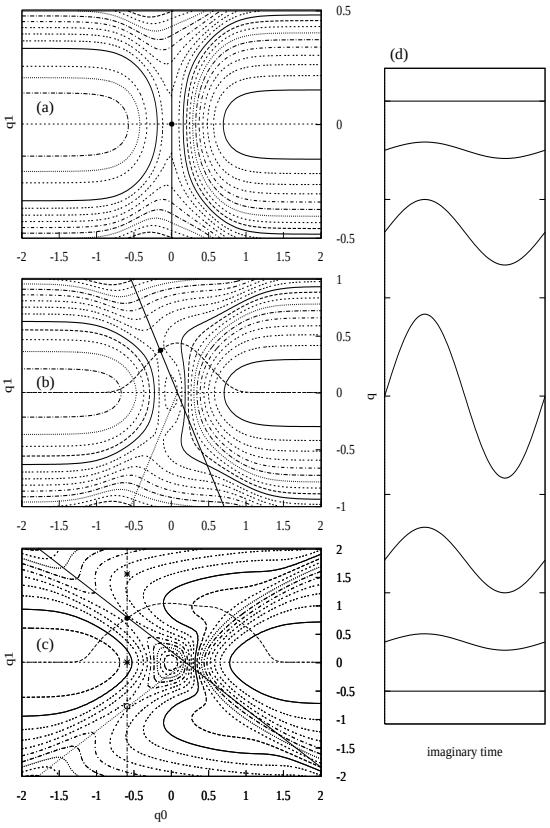

Fig. 2. – Contour plots of the Euclidean action, S_E, for an asymmetric Eckart barrier in a two-dimensional space of closed Feynman paths given by $q(\tau) = q_0 + q_1 \sin(2\pi\tau/\beta\hbar)$. The horizontal axis gives the location of the average of the path, q_0 (the 'centroid') and vertical axis, q_1 (the first non-zero Fourier component), indicates how much the paths stretch out from q_0. The dotted line at $q_1 = 0$ represents the collapsed, classical paths. The maximum along the minimum energy path, the saddle point, is shown with a filled circle. (a) $T = 300\ K$, above the crossover temperature: At this temperature, the action increases when the paths are spread open, i.e. q_1 becomes non-zero. The MAP therefore only includes collapsed paths and reduces to the MEP. (b) $T = 150\ K$, below the crossover temperature: A local maximum in $S_E(\mathbf{q})$ develops on the barrier region ($q_0 = q_1 = 0$). The projection of the MAP onto the two-dimensional space is shown with a dashed line. The MAP now includes delocalized paths, a signature of tunneling. A hyperplanar dividing surface going through the upper saddle point of the action is indicated by a thick, solid lines. This is not a good choice of a transition state because it does not include the lower saddle point (at negative q_1). A hyperplane going through the lower saddle point is shown with a dotted line. When P images are included in the discrete representation of the Feynman paths, saddle points appear in sets of P equivalent saddle points and it takes P hyperplanes to form a good transition state dividing surface. In the continuum limit, this family of hyperplanes envelopes a cone in action space. (c) $T = 50\ K$, well below the crossover temperature: Same qualitative picture as in (b) but now the cone needs to be more pointed. The vertical line indicates a dividing surface defined in the classical coordinate space (such as the dividing surface used in the centroid density approximation). Clearly, such a dividing surface would not be a good transition state. The system would be able to slide to the low action regions (shown with stars) away from the saddle point region (filled circle). (d) A plot of a few of the Feynman paths showing qualitatively (by including only two Fourier components) the variation along the MAP at temperature below T_c. The top and bottom paths, corresponding to reactant and product regions, are collapsed $q(\tau) = q_0$. But, in the intermediate, barrier region the paths stretch out because the curvature of the potential is larger than the spring constant in the Feynman paths.

Note from figure 2 that the action surface has a twofold symmetry about the $q_1 = 0$ axis. This is a reflection of the arbitrariness in parametrizing the path with τ. A change in the sign of q_1 does not change the action. When the paths are represented in a discrete way by P images in real space, the action surface has a P-fold symmetry. Given a configuration of a closed Feynman path, $\mathbf{q} = \{q^{(1)}, q^{(2)}, q^{(3)}, \ldots, q^{(P)}\}$, a relabeling of the images, such as $\{q^{(P)}, q^{(1)}, q^{(2)}, \ldots, q^{(P-1)}\}$ does not change the action. Therefore, for any saddle point configuration of the path, there are other $P-1$ saddle point configurations that simply correspond to relabeling of the images, an operation that leaves the value of the action unchanged. In the limit of a continuous representation of the Feynman paths ($P \to \infty$), there is a continuum of saddle points. An effective transition state dividing surface should be such that the system is confined to the region around all of the P saddle points.

An important concept in classical TST is the minimum energy path (MEP) connecting reactants and products. At any point along the path, the potential is at a minimum with respect to all directions perpendicular to the path. An alternative way of describing the MEP is that it follows the steepest descent in potential energy down from the saddle point both in the direction towards reactants and in the direction towards products. Letting $, _s$ denote a point on the path, where s is a parameter going from zero at the potential energy minimum in the reactant region to unity at the product minimum, the MEP satisfies

$$\frac{d}{ds}, _s = \frac{-\nabla_q V(, _s)}{|\nabla_q V(, _s)|} \tag{7}$$

subject to the additional boundary condition that the path goes through the saddle point. The MEP is the path of maximal statistical weight in the sense that the statistical weight $exp(-V(q)/kT)$ is maximal with respect to all displacements perpendicular to the path. The MEP is, therefore, a natural choice for a reaction path and the parameter s a natural choice of a reaction coordinate for the transition. There is a clear generalization of this to quantum systems, a path, $\mathbf{\Gamma}_s$ (recall, bold face is used for NP dimensional vectors), through action space which has maximal statistical weight $exp(-S(\mathbf{q})/\hbar)$ with respect to displacements perpendicular to the path in action space (see figures 2b and 2c). Such a 'minimum action path' (MAP), can be defined as

$$\frac{d}{ds}\mathbf{\Gamma}_s = \frac{-\nabla_q S_E(\mathbf{\Gamma}_s)}{|\nabla_q S_E(\mathbf{\Gamma}_s)|} \tag{8}$$

subject to the boundary condition that the path goes through a saddle point on the action surface. Above the crossover temperature (figure 2a), the MAP reduces to the MEP. We will choose s as the 'reaction coordinate' of the quantum transition. It is a parameter that gradually shifts the quantum system from reactants to products as s goes from 0 to 1. Figure 3 shows the MAP for the Eckart barrier corresponding to $T = 50K$. The MAP was found by constructing a sequence of 81 closed Feynman paths, where in addition to the spring interaction between images in a given path (chosen to be appropriate for $T = 50K$), the corresponding images in adjacent Feynman paths in the string were connected by an arbitrary spring force, simply to ensure a continuous string of Feynman paths stretching from the reactant region to the product region. This 'elastic band' of closed Feynman paths was then optimized using the Nudged Elastic Band (NEB) method [20] so as to trace out the MAP. Towards the ends of the elastic band, in the reactant and product regions, the Feynman paths collapse to a point since

the forces due to the Eckart potential are very small and the Feynman springs dominate. At low enough temperature, below the crossover temperature T_c, the spring constant in the Feynman paths (eqn. 6) becomes smaller than the curvature of the potential barrier. Then, the Feynman paths open up in the barrier region as shown in figure 3. This means that tunneling becomes important.

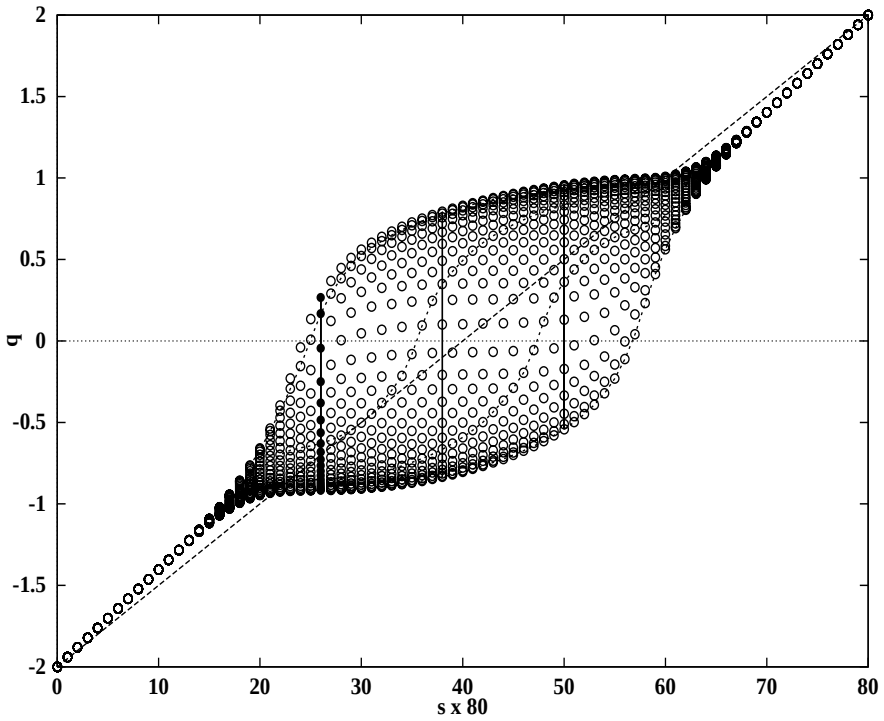

Fig. 3. – The minimum action path discretized with a total of 81 closed Feynman paths. The path was found using the Nudged Elastic Band method for the Eckart barrier (see figure 1) and Feynman springs set for $T = 50\ K$. The vertical axis gives the location of the images in the Feynman paths (each image is shown as a circle) and the horizontal axis is the reaction coordinate scaled with 80. Each of the closed Feynman paths includes $P = 20$ images. A string or 'elastic band' stretching from the reactant ($q = -2$) to the product region ($q = 2$) is formed. Corresponding images in adjacent Feynman paths are connected with springs of arbitrary spring constant (shown for two examples as small-dashed lines) to ensure continuity and equal distribution of the Feynman paths along the elastic band. The Feynman paths open up in the intermediate, barrier region (analogous to figure 2(d), except the paths only included two Fourier components in that case). The saddle point (instanton) path corresponding to the maximum action along the minimum action path is shown with filled circles (Feynman path number 26 in the elastic band).

The action along the MAP is shown in figure 1 at various temperatures. At high temperature, above T_c, the $S_E/\beta\hbar$ is identical to the potential energy curve. Below T_c, the action curve drops more and more the lower the temperature is. The saddle point on the action surface, the instanton, is the point of maximum action along each of the curves. Note that due to the asymmetry of the potential barrier, the instanton is much

closer to the reactant than the product region.

5. – The conical dividing surface of RAW-QTST

The MAP defines a 'direction' for the transition in action space. It is advantageous to use dividing surfaces that have normal vector tangent to the MAP, $\hat{\mathbf{n}}_s \equiv \mathbf{\Gamma}'_s/\|\mathbf{\Gamma}'_s\|$ (prime denotes d/ds). This ensures that when the system is confined to a dividing surface that includes the saddle point, the system remains in the saddle point region and does not slide down along the unstable mode (a normal mode corresponding to concave shape of the action surface). Since the goal is to find a bottleneck region and the free energy associated with that, it is important to constrain the system in the appropriate way.

The simplest dividing surface of this kind is a hyperplane with normal vector $\hat{\mathbf{n}}_s$. To calculate the partition function of a hyperplane, the constraint factor $\delta_{rp} \equiv \delta(\hat{\mathbf{n}}_s \cdot (\mathbf{q} - \mathbf{\Gamma}_s))$ would need to be included in the path integral, eqn. 4. However, it can be seen clearly from figure 2b and 2c, that a hyperplanar dividing surface is not a good choice for a transition state. The problem is that the hyperplane only goes through one saddle point while P equivalent saddle points will be present when P images are used in the discretization of the Feynman paths. In the continuum limit ($P \to \infty$), the Feynman paths are $q(\tau)$, and since they are closed, they satisfy $q(\tau) = q(\beta\hbar + \tau)$. The Euclidean action is invariant under relabeling of the images in the discrete representation, as discussed above, or, equivalently, using the continuous representation, $S_E[q(\tau)] = S_E[q(\tau + t)]$. This simply reflects the fact that the origin of the variable τ is arbitrary. It can be shown that the Feynman paths equivalent by this symmetry form a 'circle' in action-space [19]. For each point on the MAP, $\mathbf{\Gamma}_s$ and tangent $\hat{\mathbf{n}}_s$ there is a family of equivalent points lying on a circle $\mathbf{\Gamma}_{s,t}$ and corresponding tangents $\hat{\mathbf{n}}_{s,t}$ as the parameter t runs through the interval $0 < t < \beta\hbar$ (see figure 4).

A better dividing surface, that will lead to a better transition state, can be constructed from a family of hyperplanes defined from by the normal vectors $\hat{\mathbf{n}}_{s,t}$ and points $\mathbf{\Gamma}_{s,t}$. This family of hyperplanes envelops a cone (see figure 4). The axis of the cone consists of all collapsed paths with no spreading of the images. The set of equivalent points $\{\mathbf{\Gamma}_{s,t}\}$ is the circular intersect between the cone and a plane with normal along the axis. The calculation of the partition function of the system confined to the conical dividing surface includes integration over all the equivalent configurations within a circle $\{\mathbf{\Gamma}_{s,t}\}$. We will refer to this degree of freedom , t, as the 'zero mode'. Since the action is invariant along the circle, its contribution to the partition function can be separated out and evaluated analytically. This facilitates the numerical sampling of the remaining degrees of freedom in the Feynman paths which will, eventually, be used to calculate the free energy differences. The remaining degrees of freedom represent a NP-2 dimensional wedge of the cone (see figure 4). The contribution of the zero mode to the partition function is [19] $Q_0^{loc}(\mathbf{q}) \equiv \beta\hbar \ (\hat{\mathbf{v}}_s \cdot \dot{\mathbf{q}})$ where $\hat{\mathbf{v}}_s \equiv \dot{\mathbf{\Gamma}}_s/\|\dot{\mathbf{\Gamma}}_s\|$ and $\dot{\mathbf{q}} = d\mathbf{q}/d\tau$. The cone dividing surface partition function, Q_s, can then be evaluated from

$$Q_s = \left(\frac{\mu}{2\pi\hbar\Delta\tau}\right)^{NP/2} \int e^{-S_E(\mathbf{q})/\hbar}\ Q_0^{loc}(\mathbf{q})\ \delta_{rp}\ \delta_0\ \mathcal{D}q[\tau]. \tag{9}$$

where $\delta_0 \equiv \delta(\hat{\mathbf{v}}_s \cdot (\mathbf{q} - \mathbf{\Gamma}_s))$. The constraint, $Q_0^{loc}\delta_{rp}\delta_0$, specifies the NP-2 dimensional wedge of the dividing surface cone.

The transition state in our theory is chosen to be the cone corresponding to the tightest statistical bottleneck, i.e. the cone with maximum free energy [21]. The cal-

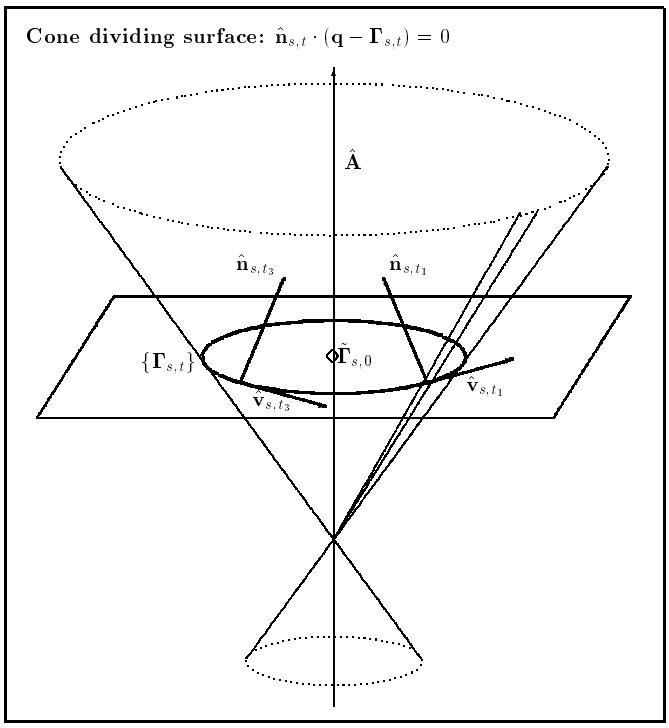

Fig. 4. – The dividing surface cone. The cone is enveloped by the hyperplanes satisfying $\hat{\mathbf{n}}_{s,t} \cdot (\mathbf{q} - \mathbf{\Gamma}_{s,t}) = 0$ for each value of the parameter t in the interval $[0, \beta\hbar]$. The set of Feynman paths $\mathbf{\Gamma}_{s,t}$ form a 'circle' in action space. The circle is centered at the centroid, $\tilde{\mathbf{\Gamma}}_{s,0}$ on the axis of the cone. The unit, local velocity, $\hat{\mathbf{v}}_{s,t} \equiv \dot{\mathbf{\Gamma}}_{s,t}/\|\dot{\mathbf{\Gamma}}_{s,t}\|$, is shown for $t = t_1$ and $t = t_3$ as well as the normal vector tangent to the Feynman paths $\hat{\mathbf{n}}_{s,t} \equiv \mathbf{\Gamma}'_{s,t}/\|\mathbf{\Gamma}'_{s,t}\|$ (prime denotes d/ds). When evaluating the partition function for the dividing surface, the zero mode, t, can be integrated out analytically, and the numerical, statistical sampling is carried out over a NP-2 dimensional wedge of the cone, chosen here to include the point $\mathbf{\Gamma}_{s,t_1}$.

culation of the free energy is carried out by evaluating the reversible work of shifting the dividing surface from the reactant region towards products, using the reaction coordinate, s, to parametrize the progression. Since the statistical weight of a Feynman path configuration in the wedge of the cone is $exp(-S_E(\mathbf{q})/\hbar)\ Q_0^{loc}(\mathbf{q})$ it is convenient to define an effective potential

$$V_{eff}(\mathbf{q}) \equiv -k_B T\ \ln\left(e^{-S_E(\mathbf{q})/\hbar} Q_0^{loc}(\mathbf{q})\right) \tag{10}$$

and the resulting effective force $\mathbf{F}_{eff}(\mathbf{q}) = -\nabla_q V_{eff}$. This simplifies the notation of the free energy expression. The change in the free energy as the dividing surface is shifted along the reaction coordinate s is [19]

$$\mathcal{F}'_s \ = \ -\Big\langle \mathbf{F}_{eff} \cdot \{\hat{\mathbf{n}}_s - (\hat{\mathbf{n}}_s \hat{\mathbf{n}}'_s + \hat{\mathbf{v}}_s \hat{\mathbf{v}}'_s) \cdot (\mathbf{q} - \mathbf{\Gamma}_s)\} - \frac{\hat{\mathbf{v}}'_s \cdot \dot{\mathbf{q}}}{\beta \hat{\mathbf{v}}_s \cdot \dot{\mathbf{q}}} \Big\rangle. \tag{11}$$

The first term is due to translation of the dividing surface along the reaction coordi-

nate. The remaining terms account for rotation in the $\mathbf{n}_s$ and $\mathbf{v}_s$ directions. In the numerical sampling, we start with the MAP $\mathbf{q} = \mathbf{\Gamma}_s$ obtained from the NEB calculation, and then run classical 'dynamics' simulations for a discrete set of values of s where the system is constrained by $\delta_{rp}\delta_0$ and the force is the negative gradient of V_{eff} (given by eqn. 10). This gives the required statistical sampling. The effective force includes $\nabla_q \left(-\hbar \ln Q_0^{loc}(\mathbf{q})\right)$ which points towards paths with larger Q_0^{loc} and is infinite wherever $Q_0^{loc} = 0$. This 'phantom' force arises from the fact that only a wedge of the dividing surface cone is sampled and it guarantees that $Q_0^{loc} > 0$.

The transition state, $s^\ddagger$, is the cone which gives a maximum in the free energy function $\mathcal{F}_s$. The free energy barrier is $\Delta\mathcal{F} = \int_R^\ddagger \mathcal{F}'_s ds = -(1/\beta)\, \ln Q_{s^\ddagger}/Q_{s_R}$ and the rate constant is given by

$$Q_\parallel^R \; k^{QTST} \;=\; \nu \; e^{-\beta\Delta\mathcal{F}} \tag{12}$$

where ν is a weakly temperature dependent prefactor, given below, and $Q_\parallel^R \equiv Q_R/Q_{s_R}$. Here s_R refers to a dividing surface located in the reactant region, s=0.

6. – The prefactor for RAW-QTST

The discussion above focused on the definition of the quantum transition rate and a method for calculating the free energy barrier. This is the most important factor determining the transition rate. But, in order to obtain an estimate of the rate constant, it is also necessary to estimate the flux out of the transition state. For this purpose, we use the 'ImF' formalism which has been shown to work well for classical as well as low temperature quantum systems [5, 22, 24, 25]. It can be related to the rigorous flux-flux correlation function expression of the rate [13, 27]. We expand the dividing surface free energy around $s^\ddagger$ up to second order in s. This represents an unstable state. A total free energy, $exp(-\beta\mathcal{F}) = \int exp(-\beta\mathcal{F}(s))\; ds$, can be defined for this unstable state by rotating the integration contour to the imaginary s axis. The decay rate of the state is then directly related to imaginary part of the free energy[22]. The resulting prefactor for RAW-QTST is [26]

$$\nu \;=\; \frac{\phi}{\beta\hbar}\sqrt{\frac{2\pi}{\beta|\mathcal{F}''(s^\ddagger)|}} \tag{13}$$

where ϕ is the Affleck switching factor, $\phi = 1$ for $T < T_c$ and $\phi = T_c/T$ for $T > T_c$ [25]. With this prefactor, RAW-QTST becomes variational classical transition state theory [2] in the high temperature, classical limit [27].

At sufficiently low temperature, the statistical sampling of Feynman paths is dominated by regions of small S_E. A harmonic approximation obtained by expanding $S_E(\mathbf{q})$ around the MAP can then be used. The saddle point of the action surface, i.e. the maximum of the action along the MAP, becomes the bottleneck. This is analogous to the situation in classical systems where the saddle point of the potential energy surface becomes the bottleneck at low temperature. In fact, TST is most often applied within the harmonic approximation where a normal mode expansion around the saddle point and the reactant minimum is used to evaluate the partition functions [28, 29]. A quantum theory based on an analogous harmonic expansion of the action has been developed [23, 24]. The dominant, exponential variation of the rate with temperature is given by the action at the saddle point while the prefactor is given by the eigenvalues of the normal modes, except the zero mode which has to be treated separately. The saddle point

Feynman path is often referred to as the 'instanton' and the harmonic rate theory as 'instanton theory' [24]. Being a stationary point of the action, the instanton is typically described in terms of a classical trajectory on the inverted potential. Instanton theory, which is known to give accurate rate estimates at low temperature, can be obtained from RAW-QTST by taking the harmonic limit. The high temperature limit of RAW-QTST is variational classical transition state theory, which is known to work well for classical systems. The high temperature and low temperature harmonic limits of RAW-QTST are therefore known to give good rate estimates. At all temperatures, RAW-QTST treats tunneling on an equal footing with over-the-barrier transitions and includes full anharmonic effects in both the transition and reactant states. Above T_c, where tunneling is unimportant, our theory reduces to variational centroid density theory [14], but below T_c the centroid variable does not play any special role.

7. – Application of RAW-QTST to a test problem

We now discuss the results obtained when the RAW-QTST method is applied to the one-dimensional Eckart barrier shown in figure 1 and discussed above (see also figures 2 and 3).

For this simple test problem, the exact rate can be evaluated (see ref. [17]) and the temperature dependence shows the characteristic crossover from a classical to a quantum regime as the temperature is reduced, as shown in figure 5. The rate calculated by the RAW-QTST method is found to give good agreement with the exact rate over the whole temperature range as shown in figure 5. At just below the crossover temperature, T_c, the centroid density theory gives similar results. But, at lower temperature the results of the centroid density calculation become unphysical, the calculated rate constant increases as temperature is further reduced (even though the dividing surface is adjusted in these calculations to minimize the rate at each temperature). The problem is that the dividing surface defined in terms of the centroid coordinate becomes too weak a constraint and the system can avoid the bottleneck region by sliding down towards reactants or products along the unstable mode at the saddle point (the centroid density dividing surface, as well as any dividing surface defined only in terms of the N classical coordinates, corresponds to a vertical line figure 2(a-c)) [16]. This problem with the centroid density approximation does not arise in symmetric systems because then the unstable mode at the saddle points happens to be in the direction of the centroid coordinate (q_0 axis in figure 2). The instanton theory is very good at low temperature but overestimates the rate at higher temperatures, as can be expected, and breaks down as the temperature approaches T_c. [5].

The RAW-QTST method is not only applicable to small test problems. It has already been applied to a large system, the associative desorption of H_2 from a Cu(110) surface, a transition involving the displacement of two quantum particles and thermal averaging over a couple of hundred other quantum and classical particles. The results of those calculations have already been described elsewhere [18].

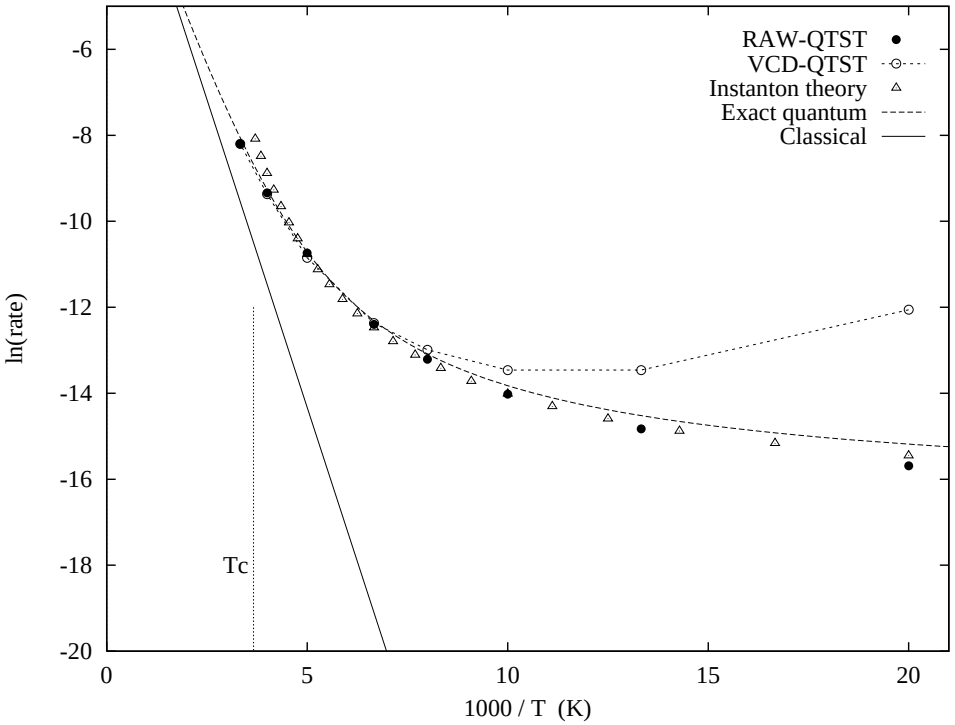

Fig. 5. – The calculated transition rate for the asymmetric Eckart barrier. At low temperature, below 100 K, the results of the variational centroid density approximation (VCD-QTST) show an unphysical increase in the rate as temperature is reduced. At high temperatures, near the crossover temperature $T_c = 273$ K, the instanton results overestimate the rate. The results of the RAW-QTST calculations, which include full anharmonicity, agree well with the exact results, coincide with the centroid density results at high temperature, and are close to the harmonic, instanton limit at low temperature.

* * *

We gratefully acknowledge helpful discussions with Giovanni Ciccotti, Bruce Garrett and Horia Metiu. This work was supported by the Division of Chemical Sciences, Office of Basic Energy Sciences, U.S. Department of Energy under grant No. DE-FG06-91ER14224 (G.M. and H.J.) and under Contract No. DE-AC06-76RLO 1830 with Battelle Memorial Institute which operates the Pacific Northwest National Laboratory (G.S. and D.M.). G.M. was a Hertz foundation graduate fellow.

REFERENCES

[1] P. Pechukas, in 'Dynamics of Molecular Collisions', part B, ed. W. H. Miller (Plenum Press, N.Y. 1976).
[2] D.G. Truhlar, B.C. Garrett and S.J. Klippenstein, J. Phys. Chem., **100**, 12771 (1996).
[3] J. C. Keck, *Adv. Chem.* **13**, 85 (1967).
[4] G. Mills, H. Jónsson and G. K. Schenter, *Surf. Science*, **324**, 305 (1995).

[5] V.A. Benderskii, D.E. Makarov and C.A. Wight, *Chemical Dynamics at Low Temperature* (Whiley, New York, 1994).
[6] N. Makri and D. E. Makarov, *J. Chem. Phys.*, **102** 4600 (1995).
[7] N. Makri, *Journal of Mathematical Physics*, **36** 2430 (1995).
[8] R. P. Feynman and A. R. Hibbs, *Quantum Mechanics and Path Integrals*, (McGraw Hill, New York, 1965).
[9] D. Chandler and P. G. Wolynes, *J. Chem. Phys.*, **74**, 4078 (1981).
[10] M. J. Gillan, *J. Phys. C: Solid State Phys.* **20** 3621 (1987); *Phys. Rev. Lett.*, **58** 563 (1987); *Philosophical Magazine A*, **58** 257 (1988).
[11] G. A. Voth, D. Chandler, and W. H. Miller, *J. Chem. Phys.*, **91**, 7749 (1989); J. Lobaugh and G. A. Voth, *J. Chem. Phys.*, **100**, 3039 (1994).
[12] J. Cao and G. A. Voth, *J. Chem. Phys.*, **105**, 6856 (1996).
[13] A. A. Stuchebrukhov, *J. Chem. Phys.*, **95**, 4258 (1991).
[14] M. Messina, G. K. Schenter and B. C. Garrett, *J. Chem. Phys.*, **98**, 8525 (1993); **99**, 8644 (1993).
[15] R. P. McRae, G. K. Schenter, B.C. Garrett, G. R. Haynes G. A. Voth, and G. C. Schatz, *J. Chem. Phys.*, **97**, 7392 (1992).
[16] D. E. Makarov and M. Topaler, *Phys. Rev. E*, **52** 178 (1995).
[17] M. Messina, G. K. Schenter and B. C. Garrett, *J. Chem. Phys.*, **103** 3430 (1995).
[18] G. Mills, G. K. Schenter, D. E. Makarov, and H. Jónsson, *Chem. Phys. Lett.*, **278**, 91 (1997).
[19] G. Mills, Ph.D. thesis (University of Washington, 1996).
[20] H. Jónsson, G. Mills, and K. W. Jacobsen, (this volume).
[21] This gives a systematic way of defining the transition state and ensures that instanton theory is recovered at low temperature and variational classical transition state theory at high temperature. However, this choice is not as well justified as in the classical case where a variational principle has been established.
[22] J.S. Langer, *Ann. Phys.(N.Y.)*, **41** 108 (1967).
[23] W. H. Miller, *J. Chem. Phys.*, **62** 1899 (1975).
[24] S. Coleman, in *The Whys of Subnuclear Physics*, ed. A. Zichichi (Plenum, N.Y., 1979)
[25] I. Affleck, *Phys. Rev. Lett.*, **46** 388 (1981).
[26] A similar expression for the prefactor has been used previously [12, 13, 16] except there $\mathcal{F}''$ was restricted to be along the centroid coordinate. Here, such a restriction is not made.
[27] G. Mills, G. K. Schenter, D. E. Makarov and H. Jónsson, (to be published).
[28] C.Wert and C.Zener, *Phys. Rev.*, **76** 1169 (1949).
[29] G. H. Vineyard, *J. Phys. Chem. Solids*, **3** 121 (1957).